Transfer of Satellite Rainfall Uncertainty from Gauged to Ungauged Regions at Regional and Seasonal Time Scales

LING TANG AND FAISAL HOSSAIN

Department of Civil and Environmental Engineering, Tennessee Technological University, Cookeville, Tennessee

GEORGE J. HUFFMAN

Science Systems and Applications, Inc., NASA Goddard Space Flight Center, Laboratory for Atmospheres, Greenbelt, Maryland

AU1

ABSTRACT

Hydrologists and other users need to know the uncertainty of the satellite rainfall datasets across the range of time–space scales over the whole domain of the dataset. Here, ''uncertainty'' refers to the general concept of the ''deviation'' of an estimate from the reference (or ground truth) where the deviation may be defined in multiple ways. This uncertainty information can provide insight to the user on the realistic limits of utility, such as hydrologic predictability, which can be achieved with these satellite rainfall datasets. However, satellite rainfall uncertainty estimation requires ground validation (GV) precipitation data. On the other hand, satellite data will be most useful over regions that lack GV data, for example developing countries. This paper addresses the open issues for developing an appropriate uncertainty transfer scheme that can routinely estimate various uncertainty metrics across the globe by leveraging a combination of spatially dense GV data and temporally sparse surrogate (or proxy) GV data, such as the Tropical Rainfall Measuring Mission (TRMM) Precipitation Radar and the Global Precipitation Measurement (GPM) mission dual-frequency precipitation radar. The TRMM Multisatellite Precipitation Analysis (TMPA) products over the United States spanning a record of 6 yr are used as a representative example of satellite rainfall. It is shown that there exists a quantifiable spatial structure in the uncertainty of satellite data for spatial interpolation. Probabilistic analysis of sampling offered by the existing constellation of passive microwave sensors indicate that transfer of uncertainty for hydrologic applications may be effective at daily time scales or higher during the GPM era. Finally, a commonly used spatial interpolation technique (kriging), which leverages the spatial correlation of estimation uncertainty, is assessed at climatologic, seasonal, monthly, and weekly time scales. It is found that the effectiveness of kriging is sensitive to the type of uncertainty metric, time scale of transfer, and the density of GV data within the transfer domain. Transfer accuracy is lowest at weekly time scales with the error doubling from monthly to weekly. However, at very low GV data density (<20% of the domain), the transfer accuracy is too low to show any distinction as a function of the time scale of transfer.

1. Introduction

Precipitation is arguably one of the most important components of the water cycle over land. One study shows that almost 70%–80% of the variability in the terrestrial water cycle can be explained from the spatio-temporal variability observed in precipitation over land (Syed et al. 2004). Existing missions such as the Tropical Rainfall Measurement Mission (TRMM) provide vital precipitation information for water cycle studies (Huffman et al. 2007). Furthermore, planned missions such as the Global Precipitation Measurement (GPM) mission will provide a global hydrologic remote sensing observatory to advance the use of precipitation sensing technologies in scientific inquiry into hydrologic processes (Krajewski et al. 2006). With the global and more frequent precipitation observational capability planned for GPM, such precipitation measuring satellite missions permit us to refine knowledge from physical and hydrologic models that can then be converted to local and global strategies for water resources management (Voisin et al. 2008; Hossain et al. 2007). (Hereafter, because our focus is on liquid precipitation, the term

Corresponding author address: Dr. Faisal Hossain, Department of Civil and Environmental Engineering, Tennessee Technological University, 1020 Stadium Dr., Box 5015, Cookeville, TN 38505. E-mail: fhossain@tntech.edu

''rainfall'' will be used as shorthand for ''precipitation'' for convenience.)

However, a crucial challenge in advancing satellite rainfall-based surface hydrologic prediction, is the need to bridge the scale incongruity between overland hydrologic processes that evolve at small scales (i.e., <1 h and <5 km) and operational satellite precipitation datasets that will always be restricted to coarser scales from passive microwave sensors (i.e., >1 h and >5 km; Hossain and Lettenmaier 2006). There are two paths that have historically been followed as a response to this scale incongruity: 1) apply satellite rainfall data available at the native scale for hydrologic prediction (e.g., Harris and Hossain 2008; Su et al. 2008; Voisin et al. 2008); and 2) apply spatial and spatiotemporal disaggregation (or downscaling) techniques to resolve satellite rainfall data at the required smaller space–time scales for hydrologic **AU2** prediction (e.g., Forman et al. 2008; Bindlish and Barros 2000). Each option leads to nonnegligible uncertainty in hydrologic simulation. In the first case, the major source of this uncertainty is due to the algorithmic and sampling uncertainty [for passive microwave (PMW) sensors] of satellite rainfall data at the native scale. In the second case, the primary source of uncertainty is due to the statistical disaggregation technique that further propagates the native scale uncertainty to subgrid uncertainty in ways that are not well understood (see, e.g., Rahman et al. 2009). Either way, hydrologists and other users need to know the uncertainty of the satellite rainfall datasets across the range of time–space scales over the whole domain of the dataset. This uncertainty can provide insightful information to the user on the realistic limits of utility that can be achieved with satellite rainfall datasets, for example for hydrologic predictability (Hong et al. 2006), on which we will focus in this paper. While representing the uncertainty structure of satellite rainfall as a function of scale against quality-controlled ground validation datasets remains a critical research problem for GPM, therein lays a paradox. Satellite rainfall uncertainty estimation requires ground validation (GV) precipitation data. On the other hand, satellite data will be most useful over ungauged regions in the developing world (Tang and Hossain 2009).

In situ rainfall information from rain gauge networks is generally considered the standard choice for GV data (Villarini and Krajewski 2007; Habib et al. 2004; McCollum et al. 2002). Such data is often referred to as ''reference'' or ''truth.'' However, in situ gauges are point measurements and unless there exists a dense network to adequately capture the space–time variability of rainfall process, its use for validating areal-averaged satellite rainfall data for surface hydrologic processes remains questionable (Ciach and Krajewski 1999). The

work of Gebremichael et al. (2003) clearly demonstrates the sensitivity of satellite rainfall uncertainty estimation to gauge density. Thus, in most regions across the globe without adequate in situ rain gauge coverage, the uncertainty associated with satellite data have been parameterized to sampling configuration of the sensors at this stage (Li et al. 1998; Huffman 1997). Some examples of this parameterization are the Global Precipitation Climatology Project (GPCP; Huffman 2005, 1997) data- **AU3** set and the TRMM Multisatellite Precipitation Algorithm (TMPA; Huffman et al. 2007) that now provide an estimate of the root-mean-squared error (RMSE) of the satellite rainfall estimates on the basis of sampling pattern and the period of rainfall accumulation of interest to the user.

While such parameterized methodologies for estimating uncertainty have been useful in providing users with a level of confidence associated with satellite rainfall estimates, such uncertainty is essentially a standard deviation measure of sampling uncertainty. Many of these uncertainty methodologies are based on the conceptual argument that uncertainty (i.e., standard deviation σ_E) **AU4** can be related directly or inversely to observation interval Δt, observation period T, spatial averaging area A, and rain rate R:

$$\sigma_E = f\left(\frac{1}{R}, \frac{1}{A}, \frac{\Delta t}{T}, \text{parameters}\right), \quad (1)$$

as expressed by Steiner et al. (2003), among others. **AU5** In many cases, the functional form of this ''predicted'' uncertainty is not benchmarked to the realities of the ground observations and hence may not provide a reasonable assessment in indicating the expected reliability for water cycle studies (Gebremichael et al. 2010). Recently, several other parameterized methodologies have evolved based on data assimilation approaches [e.g., Kalman filtering in the Global Satellite Mapping of Precipitation (GSMaP) product of Ushio et al. 2009]. In these approaches, an estimate of uncertainty that is available is essentially related to the methodology of the filtering technique and does not necessarily indicate the actual level of agreement with GV rainfall data. In some instances, however, the uncertainty is estimated by comparing the output of a wide-coverage technique [such as infrared (IR) advected PMW] to a more localized but higher accuracy product (such as PMW only; Ushio et al. 2009).

There now exists a sufficient body of knowledge on uncertainty metrics and models that we should consider a transition to a more hydrologically relevant framework in anticipation of the satellite data-rich scenario of GPM. Although existing uncertainty metrics and
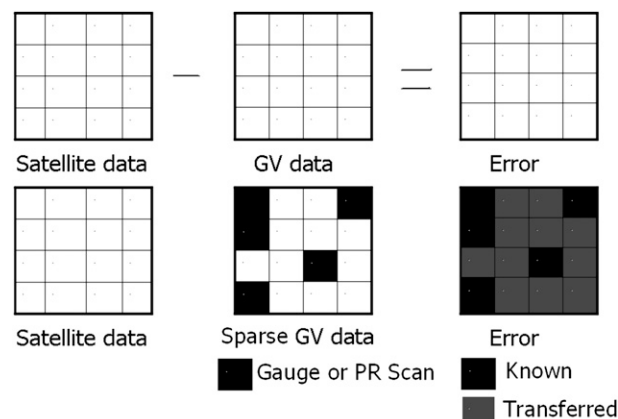
FIG. 1. Conceptual rendition of the idea of ''transfer'' of uncertainty information from a gauged (GV) location to an ungauged (non GV) location. (top) The notion of ''uncertainty'' of satellite rainfall data (in this case, the scalar deviation of magnitudes is termed uncertainty although there are many other types of uncertainty). (bottom) The known uncertainty [(middle) derived from GV sites shown in black] would be transferred to the non-GV [(right) ungauged sites shown in gray]. [Reprinted from Tang and Hossain (2009).]

AU16

uncertainty models represent an important first step, most treat uncertainty as a single measure representative for a large space and time domain. This unidimensional uncertainty measure is invariably the standard deviation of uncertainty [e.g., Eq. (1)]. However, a satellite rainfall product with a σ_E of X mm h^{-1} over a large space–time domain can be represented by a multiplicity of distinct spatiotemporal patterns of rainfall, each having a distinct response in surface hydrology (see, e.g., Lee and Anagnostou 2004).

What is therefore needed now for advancing the hydrological application of GPM is a practical methodology that can routinely ''transfer'' a set of hydrologically relevant uncertainty metrics from locations/regions having GV-based values to ungauged regions for improving water cycle studies or water resources management. Here, transfer is akin to spatial interpolation at non-sampled locations (grid boxes) using measurements from sampled but sparse locations (grid boxes). Figure 1 provides a conceptual rendition of this idea of the transfer of uncertainty based on the concept of spatial interpolation (reprinted from Ling and Hossain 2009).

F1

AU6

This paper analyzes the open issues for developing an appropriate uncertainty transfer scheme that can routinely estimate various uncertainty metrics across the globe by leveraging a combination of spatially dense GV data and temporally sparse surrogate (or proxy) GV data from sources such as the TRMM-like Precipitation Radar (PR) sensor anticipated during the GPM era. The
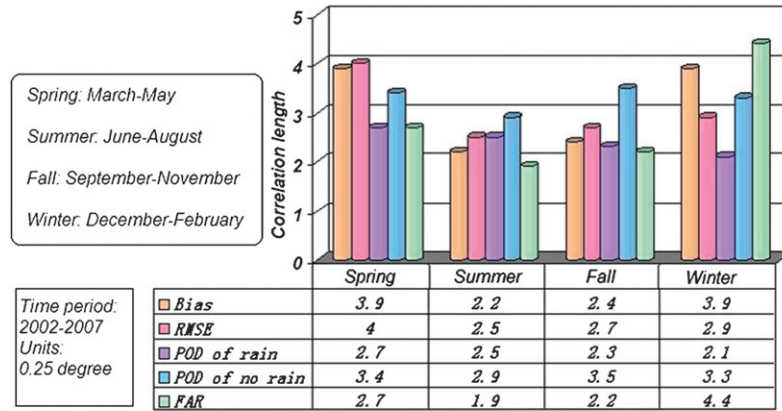
TMPA products 3B42RT and 3B41RT (Huffman et al. 2007) over the United States spanning a record of 6 yr are used as a representative example of satellite rainfall. The paper presents a probabilistic analysis of sampling offered by the existing constellation of precipitation-relevant satellite PMW sensors to understand the current and expected spatial coverage during the GPM era. A commonly used spatial interpolation technique (kriging), that leverages the spatial correlation of rainfall estimation uncertainty, is then investigated for its effectiveness. This effectiveness is cast in the context of the expected sparseness in GV data expected from TRMM and GPM missions. Finally, important issues needing closure are summarized on the basis of our investigation of the transfer of satellite rainfall uncertainty from GV to non-GV regions. To avoid confusion among readers, hereafter, the terms ''uncertainty'' or ''uncertainty metric'' will be used to define the quality indices of the satellite rainfall estimate derived at GV locations [such as bias, RMSE, and probability of detection (POD)]. The terms ''error'' or ''transfer error'' will be used specifically to define the quality of the transfer (spatial interpolation) process of uncertainty metrics at non-GV locations.

2. Spatial correlation of satellite rainfall uncertainty

The initial requirement for an effective transfer (spatial interpolation) scheme is the presence of a quantifiable spatial structure (or spatial correlation) in the variable being transferred. Therefore, we first investigated the presence of spatial correlation of satellite rainfall uncertainty. First, to minimize the error of the GV rainfall data, we used the National Centers for Environmental Prediction (NCEP) 4-km Stage IV Next Generation Weather Radar (NEXRAD) rainfall data that is adjusted to precipitation gauges and is conveniently available as a quality-controlled data mosaic over the United States (Lin and Mitchell 2005; Fulton et al. 1998). TMPA's near-real-time satellite rainfall data products from PMW-calibrated IR and merged PMW–IR estimates (labeled 3B41RT and 3B42RT, respectively; Huffman et al. 2007) were used as the satellite rainfall data. The data for GV and satellite rainfall data spanned 6 yr from 2002 to 2007. The NEXRAD Stage IV GV rainfall data were first remapped to 0.25° 3-hourly resolution for consistency with the native scale of the satellite rainfall products. 3B41RT data were also remapped at the 3-hourly time scale. After a thorough quality assessment (QA) and quality control (QC), the datasets were organized by season and various regions for the years 2002–07.

3B41RT Analysis on Spatial Structure per Season
(Correlation Length)

Spring: March-May

Summer: June-August

Fall: September-November

Winter: December-February

Time period: 2002-2007 Units: 0.25 degree

	Spring	Summer	Fall	Winter
Bias	3.9	2.2	2.4	3.9
RMSE	4	2.5	2.7	2.9
POD of rain	2.7	2.5	2.3	2.1
POD of no rain	3.4	2.9	3.5	3.3
FAR	2.7	1.9	2.2	4.4

3B42RT Analysis on Spatial Structure per Season
(Correlation Length)

Spring: March-May

Summer: June-August

Fall: September-November

Winter: December-February

Time period: 2002-2007 Units: 0.25 degree

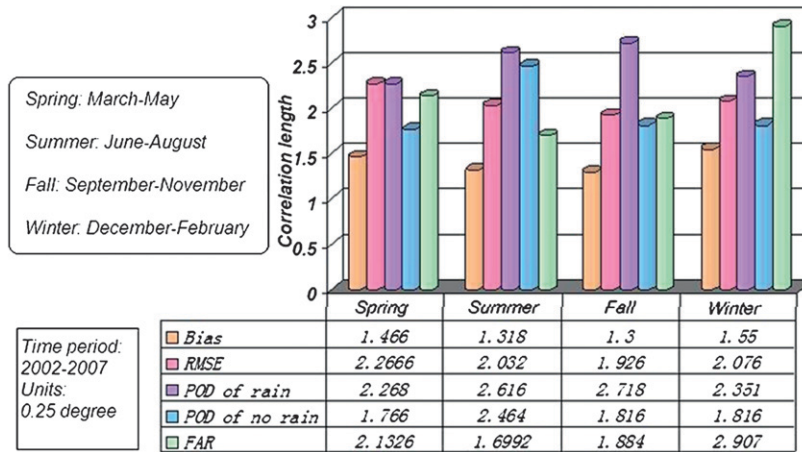|	Spring	Summer	Fall	Winter
Bias	1.466	1.318	1.3	1.55
RMSE	2.2666	2.032	1.926	2.076
POD of rain	2.268	2.616	2.718	2.351
POD of no rain	1.766	2.464	1.816	1.816
FAR	2.1326	1.6992	1.884	2.907

FIG. 2. Correlation length of uncertainty metrics at climatologic time scales for (top) 3B41RT and (bottom) 3B42RT as a function of season. Note the distance unit is 0.25° grid boxes (~25 km). (from left to right) The vertical bars for each season are shown in order as Bias, RMSE, POD rain, POD no-rain, and FAR (Tang and Hossain 2009).

To study how the satellite rainfall uncertainty is spatially dependent (or correlated), Tang and Hossain (2009) derived the spatial correlograms for each uncertainty metric using the TMPA dataset described above. Herein, the correlation length (CL), where the autocorrelation dropped to $1/e$ (e-folding distance), was first computed. Next, the empirical semivariograms were derived and then idealized as exponential semivariogram functions:

$$\gamma(h) = c_0 + c(1 - e^{-h/a}), \qquad (2)$$

where $\gamma(h)$ is the semivariance at spatial lag "h," c_0 represents the nugget variance (i.e., the minimum variability observed or the "noise" level at a separation distance of zero), c is the sill variance (when spatial lag is infinite), and a is the correlation length. Figure 2 provides a summary of the "climatologic" correlation length (e-folding distance) by season for various uncertainty metrics of the satellite rainfall products such as POD for rain, POD for no rain, false-alarm ratio (FAR), RMSE, and bias. Herein, climatologic refers to the mean error derived from the entire 6 yr of data. The appendix provides the mathematical formulation for the error metrics.

Figure 2 clearly demonstrates that, at the climatologic (long term) time scale, satellite rainfall uncertainty can

F2

have distinct spatial organization that can be leveraged for spatial interpolation. The correlation lengths for a given uncertainty metric as a function of season appear to be at least 3–5 (0.25°) TMPA grid boxes long. As a rule of thumb, this indicates that the transfer of error from sampled locations may be effective up to 4 grid boxes (~100 km) away. Another interesting feature that is revealed in this figure is the significantly higher correlation lengths (and spatial organization) observed for 3B41RT than 3B42RT. This can be traced to the sources of the specific satellite estimates: 3B41RT is uniformly computed using a calibration of IR brightness temperatures to a combined PMW estimate. The statistics of the uncertainty are spatially very homogenous since they originate from a single probability distribution at regional scales. On the other hand, 3B42RT uses a variety of PMW rainfall estimates with gaps filled during a 3-h sampling period with the 3B41RT estimate "as is." This fill-in causes the 3B42RT data to draw on two different probability distributions in space for uncertainty statistics (IR and PMW); the increased spatial heterogeneity in the uncertainty structure leads to a shorter correlation length. This analysis shows that any uncertainty transfer scheme should benefit from improvements in the 3B42RT product to make it statistically more homogenous in space.

3. Spatial coverage offered by current constellation of PMW sensors

Having observed a distinct spatial organization of uncertainty, we also need to understand the space–time dimension that is implicit in the concept of real-time uncertainty transfer over non-GV regions. The space dimension pertains to the regions with spatially sparse GV data due to inadequate in situ gauge data (such as that shown in Fig. 1), which are, of course, recorded at fixed positions. The time dimension pertains to the temporally sparse case of using the most accurate rainfall source currently available from space, such as the orbiting TRMM PR as "proxy" GV data, over regions where there is no ground-based GV data. Depending on how we define GV data, there can be several types of GV "voids" where uncertainty information will be need to be estimated for GPM. For example, if we rely on the "conventional" ground source for GV data, voids will be represented by large and stationary regions having little or no instrumentation. On the other hand, if a proxy for GV is defined from orbiting sensors, such as the TRMM PR, or even a highly accurate PMW sensor, then voids will be numerous grid boxes dynamically changing in location with each satellite orbit.

The left panels of Fig. 3 shows the probability of a 3B42RT grid box (0.25°) having a conical-scanning PMW overpass [comprising either the TRMM Microwave Imager (TMI), Special Sensor Microwave Imager (SSM/I), or the Advanced Microwave Scanning Radiometer (AMSR)] in 3-, 6-, and 24-h windows. In the right panels of Fig. 3, the probability of a 3B42RT grid box having a TMI scan is shown. These probability maps were created using a 100-day period of any PMW sensor from the 2007–08 period. It is clear from the maps that the spatiotemporal dynamics of the location of PMW scans is strongly sensitive to the accumulation periods of hydrologic relevance and one that must be investigated carefully in order to identify how an uncertainty transfer scheme may work using proxy-GV data.

At time scales of 3–6 h, there are vast regions lacking conventional surface GV data in the tropics of Africa, Asia, and South America where the probability of having a PMW scan is less than 50% (Fig. 3). This makes the estimation of uncertainty through transfer from GV regions at these locations more important for hydrologic applications. While GPM may improve the coverage of PMW scans, such large voids with a low probability for a PMW scan will still remain over these regions due the continued dependence on polar-orbiting sensors. Since gauge-based GV is sparse for these tropical regions at hydrologic scales, proxy GV data from space-borne sensors (such as that expected from the GPM dual-frequency precipitation radar) may be one of the few ways to explore if the transfer of uncertainty is realistic. For the higher-latitude land regions (which comprise mostly the industrialized world with reasonably gauged fixed-location GV instrumentation), the uncertainty could be transferred from the stationary GV regions. The right panels of Fig. 3 also show that the probability of having a TMI scan also happens to be lowest (0.1–0.2 in 3 h) over the tropical regions. However, over a 24-h time period there is considerably higher probability of having such a scan (~0.7–0.8). This implies that the practicable time scale for transferring uncertainty metrics over the tropics from a sun-asynchronous PMW sensor is at least 24 h.

4. Transfer of uncertainty by spatial interpolation

Tang and Hossain (2009) recently showed that most uncertainty metrics (such as bias and POD) are amenable to the transfer from gauged to ungauged locations using spatial interpolation at climatologic (6-yr average) time scales. The method of ordinary kriging (OK) was used for testing the transfer of uncertainty metrics. The OK is the most common (and one of the simplest) spatial interpolation estimator used to find the best linear
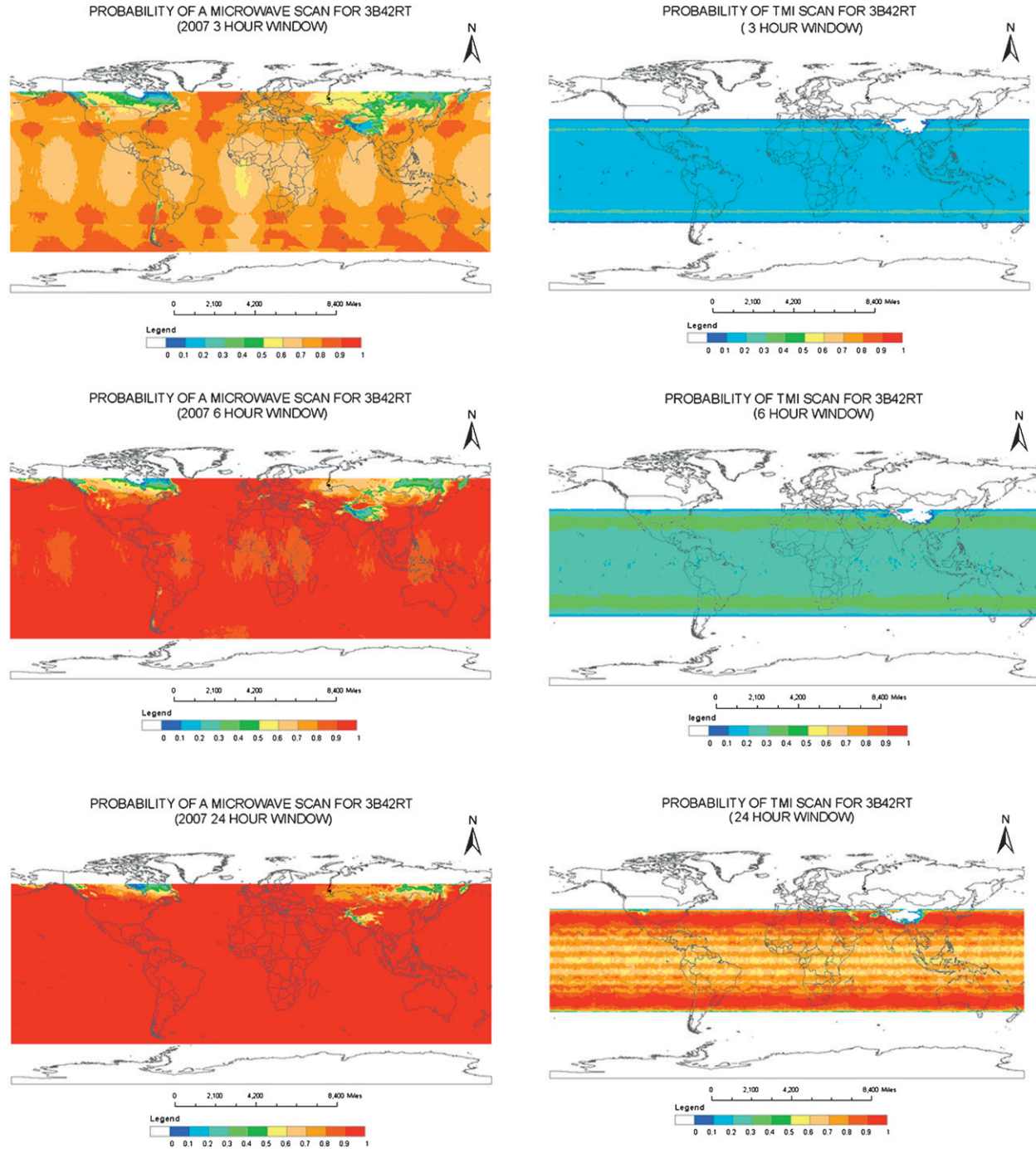
FIG. 3. (left) Probability of a 3B42RT 0.25° grid box having a PMW scan from either TMI, SSM/Is, or AMSR for (top) 3-, (middle) 6-, and (bottom) 24-h periods. (right) As at (left), but for TMI only.

unbiased estimate of a second-order stationary random field with an unknown constant mean as follows:

$$\hat{Z}(x_0) = \sum_{i=1}^{n} \lambda_i Z(x_i), \qquad (3)$$

where $\hat{Z}(x_0)$ is the kriging estimate at location x_0; $Z(x_i)$ is the sampled value at location x_i; λ_i is the weighting factor for $Z(x_i)$ (summing to 1 over all i), and n is the number of sampled (known) locations. Kriging methods have already been used for spatial interpolation of precipitation
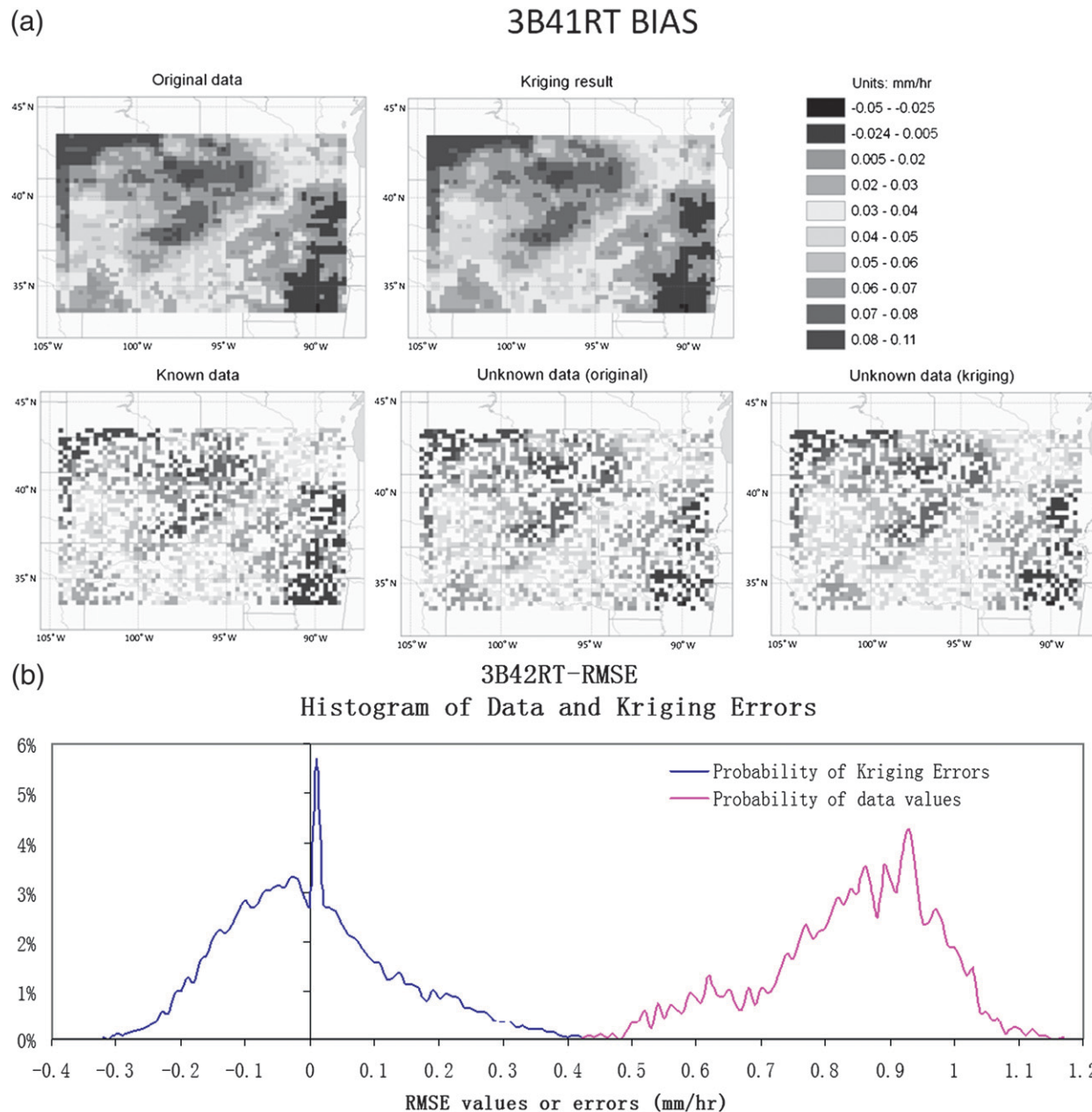
AU17   FIG. 4. (a) Transfer of bias of 3B41RT from gauged to ungauged locations. (top left) The true field of uncertainty in bias based on 6 yr of data. (bottom left) The randomly selected 50% of the region for computation of the empirical variogram and correlation length. (bottom middle) The other 50% of the region that was assumed to have no GV. (bottom right) The estimation of the bias at the non-GV grid boxes using ordinary kriging. (b) Histograms of kriging error and actual error for FAR over ungauged grid boxes. Here, kriging error (black) is defined as the difference between transferred (or kriged) FAR and the actual FAR derived from GV data. The actual GV-based FAR is shown in pink.

from point gauge data with considerable success (see, e.g., Seo et al. 1990; Krajewski 1987).

Using the same 6-yr database of high-resolution satellite rainfall data from TMPA over the central United States, the OK method was applied to assess the effectiveness of transfer of uncertainty metrics from GV to non-GV grid boxes, using correlation as the main assessment metric. Assuming that only 50% of the region (i.e., grid boxes) was gauged (i.e., having access to GV data), OK was implemented to estimate uncertainty metrics at the other 50% of the (non GV) region. Selection of "GV" grid boxes was random and hence each

kriging realization was repeated 10 times in a Monte Carlo (MC) fashion to derive an average scenario. The semivariogram and correlation lengths were computed on the basis of the 50% of the assumed "available" data. Spatial correlograms for each uncertainty metric were derived and the CL, where the autocorrelation dropped to $1/e$, was computed. The empirical semivariograms were derived and then idealized as exponential semivariogram functions.

Tang and Hossain (2009) showed that the transfer of uncertainty metrics using kriging did not lead to wholesale changes in the pattern of the uncertainty field when compared to the true climatologic uncertainty field (see top-left and top-right panels of Fig. 4a). Overall, their assessment indicated that the transfer uncertainty metrics from a gauged to an ungauged location through spatial interpolation have merit for selected uncertainty metrics. In Fig. 4b, the histograms for "kriging error" and actual uncertainty (over ungauged grid boxes) demonstrate the accuracy of the transfer method for FAR. Here, the kriging error refers to the difference between "kriged uncertainty" and the "actual uncertainty," whereas the actual uncertainty is the "measured uncertainty." In other words, the kriging error is the estimation uncertainty while the actual uncertainty is the true dataset uncertainty. The actual GV-based uncertainty (i.e., FAR in this case) is shown in pink while the black line represents the histogram for kriging error. The histograms for the kriging error are considerably lower, by almost an order of magnitude, compared to the actual GV-based uncertainty and are almost unbiased.

However, a point to note is that the work of Tang and Hossain (2009) demonstrated the utility of transfer only at the climatologic time scales with a high degree of GV coverage (50%). Also, at the climatologic scales, the spatial structure of uncertainty can be expected to be well defined and reasonably homogenous (longer correlation lengths of uncertainty that lead to high accuracy for kriging; see Fig. 2). Furthermore, the use of the correlation measure may not necessary reflect the most rigorous assessment of accuracy for the transfer of error metrics. For example, there may be a high correlation even with a large systematic bias in the "kriged" error metric at non-GV grid boxes. In this study, we therefore explored the effectiveness of kriging at seasonal (and lower) time scales and modeled how the effectiveness of transfer is impacted by GV data coverage. We also assessed the accuracy of transfer using marginal and noncorrelation type measures.

Figure 5 shows how GV coverage (as randomly located grid boxes over a region) impacts the accuracy of the kriging-based transfer of uncertainty over the grid boxes lacking GV data for two different time scales
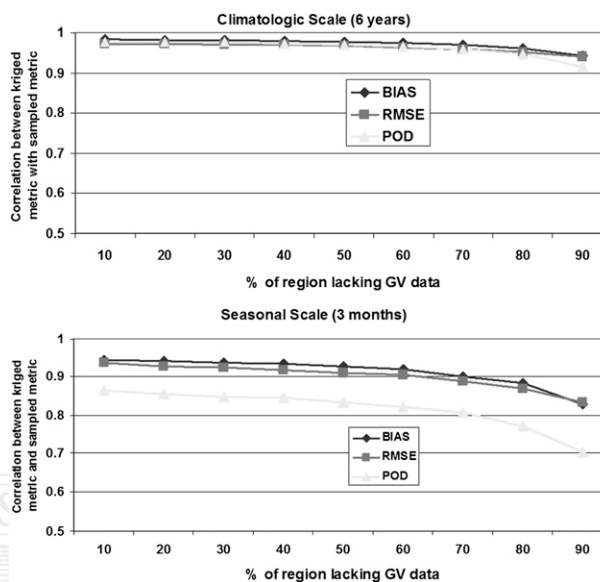

FIG. 5. Impact of GV coverage (or sparseness) on the effectiveness of uncertainty metric transfer by ordinary kriging at the (top) climatologic scale and (bottom) seasonal scale for the central United States. Computed with TMPA data collected for a 100-day period (May–August) in 2007–08.

(climatologic and seasonal in the left and right panels, respectively). The exercise was performed in a manner similar to Tang and Hossain (2009) over the central United States. The GV coverage was systematically varied from 10% to 90% and the effectiveness of kriging of uncertainty metric at locations lacking GV data was assessed using the correlation measure with in situ (sampled) uncertainty metric. For the seasonal case, the summer months of June–August in 2007 over the central United States was chosen as an example and one seasonal variogram was modeled.

The most striking feature of the GV-density study is that the effectiveness of an uncertainty transfer scheme, specifically kriging in this example, worsens considerably at low GV coverage (correlation dropping to under 0.7) as time scales shorten. Qualitatively, this result is expected, and clearly indicates that if a transfer scheme for estimating uncertainty metrics is finer than seasonal scale (ranging from 3–6-hourly to weekly–monthly), the effectiveness for uncertainty transfer would intuitively worsen further with kriging. A similar assessment can be made from Fig. 3 on the potential of kriging using dynamically located sun-asynchronous PMW scans (such as TMI) as proxy-GV data. At 3–6 h, the probability of a grid box being scanned by a sun-asynchronous TMI ranges from 0.1 to 0.4. In other words, this is equivalent to a large region having a fixed GV coverage of 10%–40%. Naturally therefore, the effectiveness of OK over

TABLE 1. Assessment of the transfer of uncertainty metrics [Eqs. (4)–(6)] at monthly time scales (for summer months of June–August).

Month	Percentage of region lacking GV data	Bias		RMSE		POD$_{RAIN}$		FAR	
		Mean error	Std dev of error	Mean error	Std dev of error	Mean error	Std dev of error	Mean error	Std dev of error
June	10	0.53	0.78	0.19	0.18	0.12	0.10	0.22	0.27
	20	0.64	0.86	0.22	0.29	0.13	0.13	0.23	0.25
	30	0.60	0.93	0.21	0.24	0.13	0.12	0.24	0.31
	40	0.66	1.00	0.22	0.24	0.13	0.14	0.22	0.26
	50	0.68	1.08	0.23	0.20	0.14	0.16	0.24	0.37
	60	0.73	1.12	0.25	0.27	0.14	0.16	0.25	0.33
	70	0.75	1.11	0.26	0.25	0.15	0.15	0.26	0.35
	80	0.85	1.24	0.27	0.30	0.16	0.16	0.28	0.40
	90	1.00	1.43	0.31	0.29	0.19	0.23	0.31	0.47
July	10	0.54	0.71	0.20	0.20	0.16	0.15	0.32	0.43
	20	0.64	0.98	0.22	0.22	0.17	0.18	0.27	0.31
	30	0.67	0.98	0.22	0.21	0.16	0.19	0.28	0.32
	40	0.61	0.85	0.23	0.24	0.18	0.22	0.31	0.41
	50	0.67	1.01	0.25	0.24	0.18	0.21	0.31	0.39
	60	0.72	1.09	0.26	0.27	0.17	0.19	0.32	0.40
	70	0.80	1.13	0.26	0.24	0.19	0.24	0.33	0.44
	80	0.87	1.32	0.30	0.34	0.21	0.25	0.35	0.48
	90	0.99	1.46	0.33	0.34	0.24	0.30	0.39	0.51
August	10	0.47	0.79	0.21	0.22	0.14	0.17	0.28	0.47
	20	0.56	0.84	0.24	0.32	0.16	0.19	0.28	0.41
	30	0.52	0.78	0.23	0.28	0.15	0.17	0.28	0.35
	40	0.62	1.00	0.24	0.30	0.15	0.17	0.27	0.34
	50	0.62	0.95	0.25	0.34	0.16	0.21	0.27	0.35
	60	0.70	1.09	0.26	0.30	0.17	0.21	0.27	0.34
	70	0.69	1.05	0.30	0.36	0.17	0.20	0.29	0.40
	80	0.78	1.16	0.36	0.49	0.18	0.20	0.31	0.43
	90	0.83	1.19	0.35	0.42	0.21	0.23	0.33	0.50

the tropics using proxy-GV data in the GPM era may not be any better at time scales shorter than a day.

To demonstrate a more rigorous level of accuracy of the interpolation scheme beyond the correlation measure, we reviewed our kriging simulations for two more scenarios: 1) transfer of the uncertainty metric at monthly time scales and 2) transfer of the uncertainty metric at weekly time scales. For each scenario, we performed a more in-depth assessment for the months of summer and weeks of June 2007. We used mean error, in place of correlation measure, to assess the accuracy of the transfer, using the following error definitions:

$$\text{Error} = \frac{[(\text{Interpolated uncertainty metric}) - (\text{Actual uncertainty metric})]}{(\text{Actual uncertainty metric})}, \quad (4)$$

$$\text{Mean error} = \langle \text{Error(non} - \text{GV grid boxes)} \rangle, \quad (5)$$

$$\text{Std dev of error} = \sigma[\text{Error(non} - \text{GV grid boxes)}]. \quad (6)$$

T1 T2   Tables 1 and 2 summarize the assessment of OK method using mean relative error [Eq. (5)] as the main assessment metric for the transfer of uncertainty metrics: BIAS, RMSE, POD, and FAR. For each uncertainty metric both the mean and standard deviation of

error of transfer is shown as measures of accuracy and precision, respectively. It is observed that, unlike correlation measure, the mean and standard deviation of error reveal a somewhat different picture on the utility of OK method. The error metric BIAS has the lowest accuracy ranging from 50% error (at 10% missing GV grid boxes) to 100% error (at 90% missing GV grid boxes) for a monthly time scale. For a weekly time scale, the mean error ranges from 80% (at 10% missing GV grid boxes) to 120% (at 90% missing GV grid boxes). On the other hand, POD, followed by RMSE

TABLE 2. As in Table 1, but at weekly time scales (for June weeks only).

Week no.	Percentage of region lacking GV data	Bias		RMSE		POD$_{RAIN}$		FAR	
		Mean error	Std dev of error	Mean error	Std dev of error	Mean error	Std dev of error	Mean error	Std dev of error
1	10	0.78	1.13	0.45	0.73	0.27	0.29	0.35	0.32
	20	0.88	1.17	0.46	0.68	0.28	0.29	0.35	0.32
	30	0.87	1.16	0.41	0.53	0.31	0.34	0.36	0.33
	40	0.86	1.15	0.48	0.76	0.33	0.35	0.35	0.31
	50	0.97	1.25	0.41	0.54	0.33	0.35	0.34	0.30
	60	0.93	1.15	0.53	0.83	0.33	0.36	0.38	0.34
	70	1.05	1.35	0.52	0.80	0.34	0.36	0.38	0.32
	80	0.98	1.15	0.56	0.81	0.37	0.38	0.38	0.33
	90	1.15	1.37	0.74	1.06	0.39	0.38	0.40	0.38
2	10	0.85	1.23	0.39	0.77	0.23	0.25	0.35	0.31
	20	0.81	1.15	0.37	0.64	0.25	0.27	0.34	0.32
	30	0.82	1.20	0.47	0.78	0.26	0.29	0.37	0.37
	40	0.80	1.19	0.47	0.77	0.27	0.31	0.37	0.37
	50	0.90	1.33	0.47	0.75	0.26	0.27	0.35	0.33
	60	0.94	1.28	0.48	0.78	0.28	0.31	0.36	0.32
	70	0.94	1.29	0.51	0.84	0.29	0.32	0.38	0.36
	80	1.08	1.45	0.61	0.96	0.29	0.33	0.38	0.38
	90	1.11	1.46	0.68	1.06	0.31	0.38	0.40	0.37
3	10	0.76	1.04	0.42	0.56	0.28	0.33	0.31	0.28
	20	0.80	1.25	0.50	0.77	0.28	0.29	0.32	0.29
	30	0.79	1.25	0.54	0.91	0.31	0.34	0.33	0.30
	40	0.82	1.19	0.52	0.80	0.32	0.37	0.32	0.29
	50	0.83	1.18	0.55	0.93	0.31	0.33	0.32	0.32
	60	0.86	1.26	0.52	0.75	0.32	0.36	0.33	0.32
	70	0.94	1.32	0.58	0.90	0.32	0.34	0.33	0.33
	80	0.98	1.30	0.60	0.88	0.35	0.38	0.34	0.35
	90	1.09	1.43	0.73	1.16	0.39	0.44	0.39	0.38

and FAR, have the highest accuracy for transfer of error metrics at both time scales according the mean relative error measure. As expected, the precision of the kriging-based transfer scheme degrades at shorter time scales. At very low GV coverage (<20%) the standard deviation of transfer error is high (>100%), indicating poor performance of the OK method regardless of the time scale at which the uncertainty metrics are transferred.

5. Conclusions

Current open issues on uncertainty transfer

In light of the impact of GV coverage and the time scale on effectiveness of uncertainty transfer, we now need to consider the following: 1) explore other techniques for transfer that are more sophisticated than ordinary kriging; and 2) understand how we can leverage the methodological error estimate that is routinely available from uncertainty models such as Huffman (1997) and the Kalman filtering techniques that many satellite

rainfall data algorithms use (e.g., Ushio et al. 2009). In our interpolation method, the spatial structure of rainfall has not been used alongside that of estimation uncertainty. Because the two (rainfall and its estimation uncertainty) are related, it may be worthwhile to pursue cokriging-type conditional interpolation schemes that leverage existing information on the satellite rainfall distribution as an extra constraint.

Also, for spatial interpolation methods, we should keep in mind that traditional geostatistical tools are pattern filling methods based on the spatial correlation exhibited by two points in space separated by a lag h. The variogram computed using this two-point geostatistical approach may simplify the spatial patterns manifested by the complex precipitation systems and surface emissivity that dictate the accuracy of satellite rainfall products at hydrologic time scales over land. For the case of spatial interpolation of groundwater contamination, it has recently been demonstrated that the use of a highly nonlinear pattern learning technique in the form of an artificial neural network (ANN) can yield significantly superior results

under the same set of constraints when compared to the ordinary kriging method (Chowdhury et al. 2009). Thus, the use of nonlinear mapping techniques is worth an investigation.

Another aspect to keep in mind is the nature of use of each uncertainty metrics. Different users will have naturally different needs. Hydrology users engaged in flash flood or monsoonal flood forecasting will probably be more interested in the POD_{RAIN} (to understand the accuracy in estimating peak flow), FAR (to minimize false alarms in flood warnings), and BIAS (to minimize under/overestimation in river stage) for each grid box (see Harris and Hossain 2008; Hossain and Anagnostou 2004). Hydrologists engaged in continuous simulation based on soil moisture accounting for drought monitoring and water management would probably focus more on POD_{NORAIN} (to minimize uncertainty in underestimating the soil wetness and evapotranspiration) for each grid box. On the other hand, crop yield and famine forecasters would like to focus more on the seasonal bias over a large agricultural zone during the growing season as the important indicator of reliability of a satellite rainfall product (Dr. C. Funk, University of California, Santa Barbara, ????, personal communication).

Developing an uncertainty transfer scheme that is amenable to operational implementation for estimation of uncertainty metrics for satellite rainfall data over regions lacking surface GV data is a necessary requirement for current and future satellite precipitation missions to advance their hydrologic potential. Hydrologist users around the world need to have a clear understanding of the pros and cons of applying satellite rainfall data for terrestrial hydrologic applications at a given scale if the benefit of these missions is to be maximized. One way of facilitating the understanding is through the routine provision of various measures of uncertainty that are of hydrologic relevance. If this uncertainty information is provided alongside the global and more frequent precipitation observational capability planned in GPM, it will permit us to refine knowledge from physical and hydrologic models that can then be converted to local and global strategies for water resources management. Work is currently undergoing to address some of the open issues discussed above and we hope to report on them in the near future.

TABLE A1. Contingency table. HIT is defined when both satellite and GV agree on the type of event detected. MISS is when there is disagreement between satellite and GV detected events.

Truth/reference (satellite estimates)	
Rainy grid boxes	Nonrainy grid boxes
N_A (HIT)	N_B (MISS)
N_C (MISS)	N_D (HIT)

APPENDIX

Formulation of Uncertainty Metrics

Consider the 2×2 contingency table (Table A1) of hits and misses associated with satellite rainfall estimates:

Probability of Detection for Rain (POD_{RAIN}):

$$\frac{N_A}{N_A + N_B}, \tag{A1}$$

Probability of Detection for No Rain (POD_{NORAIN}):

$$\frac{N_D}{N_D + N_C}, \tag{A2}$$

False Alarm Ratio (FAR): $\dfrac{N_B}{N_B + N_A}. \tag{A3}$

The POD_{RAIN} essentially defines how often a satellite rainfall estimate is likely to correctly detect grid boxes as rainy according to the reference or ground validation data. Similarly, POD_{NORAIN} defines how often a satellite rainfall estimate is likely to correctly detect a nonrainy grid box as nonrainy according to the ground validation data.

REFERENCES

Anagnostou, E. N., 2004: Overview of overland satellite rainfall estimation for hydro-meteorological applications. *Surv. Geophys.,* **25** (5–6), 511–537.

Bindlish, R., and A. P. Barros, 2000: Disaggregation of rainfall for one-way coupling of atmospheric and hydrological models in regions of complex terrain. *Global Planet. Change,* **25,** 111–132.

Ciach, G. J., and W. F. Krajewski, 1999: Radar-rain gauge comparisons under observational uncertainties. *J. Appl. Meteor.,* **38,** 1519–1525.

Chowdhury, M., A. Alouani, and F. Hossain, 2009: How much does inclusion of non-linearity affect the spatial mapping of complex patterns of groundwater contamination? *Nonlinear Processes Geophys.,* **16,** 313–317.

Forman, B., E. Vivoni, and S. Margulis, 2008: Evaluation of ensemble-based distributed hydrologic model response with disaggregated precipitation products. *Water Resour. Res.,* **44,** W12409, doi:10.1029/2008WR006827.

Fulton, R. A., J. P. Breidenbach, D.-J. Seo, D. A. Miller, and T. O'Bannon, 1998: The WSR-88D rainfall algorithm. *Wea. Forecasting,* **13,** 377–395.

Gebremichael, M., W. F. Krajewski, M. Morrissey, D. Langerud, G. J. Huffman, and R. Adler, 2003: Uncertainty uncertainty analysis of GPCP monthly rainfall products: A data based simulation study. *J. Appl. Meteor.,* **42,** 1837–1848.

——, E. N. Anagnostou, and M. Bitew, 2010: Critical Steps for Continuing Advancement of Satellite Rainfall Applications for Surface Hydrology in the Nile River Basin. *J. Amer. Water Resour. Assoc.,* **46,** 361–366, doi:10.1111/j.1752-1688.2010.00428.x.

Habib, E., G. J. Ciach, and W. F. Krajewski, 2004: A method for filtering out rain gauge representativeness uncertainty from the verification distributions of radar and raingauge rainfall. *Adv. Water Resour.,* **27** (10), 967–980.

Harris, A., and F. Hossain, 2008: Investigating optimal configuration of conceptual hydrologic models for satellite rainfall-based flood prediction for a small watershed. *IEEE Geosci. Remote Sens. Lett.,* **5** (3), ??–??.

Hong, Y., K. Hsu, H. Moradkhani, and S. Sorooshian, 2006: Uncertainty quantification of satellite precipitation estimation and Monte Carlo assessment of the uncertainty propagation into hydrologic response. *Water Resour. Res.,* **42,** W08421, doi:10.1029/2005WR004398.

Hossain, F., and E. N. Anagnostou, 2004: Assessment of current passive microwave and infra-red based satellite rainfall remote sensing for flood prediction. *J. Geophys. Res.,* **109,** D07102, doi:10.1029/2003JD003986.

——, and D. P. Lettenmaier, 2006: Flood prediction in the future: Recognizing hydrologic issues in anticipation of the global precipitation measurement mission. *Water Resour. Res.,* **44,** W11301, doi:10.1029/2006WR005202.

——, and G. J. Huffman, 2008: Investigating uncertainty metrics for satellite rainfall at hydrologically relevant scales. *J. Hydrometeor.,* **9,** 563–575.

——, N. Katiyar, A. Wolf, and Y. Hong, 2007: The Emerging role of satellite rainfall data in improving the hydro-political situation of flood monitoring in the under-developed regions of the world. *Nat. Hazards,* **43,** 199–210.

Hou, A., G. S. Jackson, C. Kummerow, and C. M. Shepherd, 2008: Global precipitation measurement. *Precipitation: Advances in Measurement, Estimation, and Prediction,* S. Michaelides, Eds., Springer Publishers, 1–39.

Huffman, G. J., 1997: Estimates of root mean square random uncertainty for finite samples of estimated precipitation. *J. Appl. Meteor.,* **36,** 1191–1201.

——, 2005: Hydrological applications of remote sensing: Atmospheric states and fluxes—Precipitation (from satellites) (active and passive techniques). *Encyclopedia for Hydrologic Sciences,* M. G. Anderson and J. McDonnel, Eds., Wiley, ??–??.

——, R. F. Adler, M. M. Morrissey, D. T. Bolvin, S. Curtis, R. Joyce, B. McGavock, and J. Susskind, 2001: Global precipitation at one-degree daily resolution from multisatellite observations. *J. Hydrometeor.,* **2,** 36–50.

——, and Coauthors, 2007: The TRMM multi-satellite precipitation analysis: Quasi-global, multi-year, combined sensor precipitation estimates at fine scales. *J. Hydrometeor.,* **8,** 28–55.

Joyce, R. L., J. E. Janowiak, P. A. Arkin, and P. Xie, 2004: CMORPH: A method that produces global precipitation estimates from passive microwave and infrared data at high spatial and temporal resolution. *J. Hydrometeor.,* **5,** 487–503.

Krajewski, W., 1987: Cokriging radar rainfall and rain gage data. *J. Geophys. Res.,* **92** (D8), 9571–9580.

Krajewski, W. F., and Coauthors, 2006: A remote sensing observatory for hydrologic sciences: A genesis for scaling to continental hydrology. *Water Resour. Res.,* **42,** W07301, doi:10.1029/2005WR004435.

Lee, K. H., and E. N. Anagnostou, 2004: Investigation of the nonlinear hydrologic response to precipitation forcing in physically based land surface modeling. *Can. J. Remote Sens.,* **30,** 706–716.

Li, Q., R. Ferraro, and N. C. Grody, 1998: Detailed analysis of the error associated with the rainfall retrieved by the NOAA/NESDIS SSM/I algorithm. 1. Tropical oceanic rainfall. *J. Geophys. Res.,* **103** (D10), 11 419–11 427.

Lin, Y., and K. Mitchell, 2005: The NCEP stage II/IV hourly precipitation analyses: Development and applications. Preprints, *19th Conf. on Hydrology,* San Diego, CA, Amer. Meteor. Soc., 1.2. [Available online at ams.confex.com/ams/Annual2005/techprogram/paper_83847.htm.]

McCollum, J. R., W. F. Krajewski, R. R. Ferraro, and M. B. Ba, 2002: Evaluation of biases of satellite rainfall estimation algorithms over the continental United States. *J. Appl. Meteor.,* **41,** 1065–1080.

Rahman, S., A. C. Bagtzoglou, F. Hossain, L. Tang, L. Yarbrough, and G. Easson, 2009: Investigating spatial downscaling of satellite rainfall data for streamflow simulation in a medium-sized basin. *J. Hydrometeor.,* **10,** 1063–1079.

Seo, D. J., W. Krajewski, and D. Bowles, 1990: Stochastic interpolation of rainfall data from rain gages and radar using cokriging. 1: Design of experiments. *Water Resour. Res.,* **26,** 469–477.

Su, F., Y. Hong, and D. P. Lettenmaier, 2008: Evaluation of TRMM Multisatellite Precipitation Analysis (TMPA) and its utility in hydrologic prediction in the La Plata Basin. *J. Hydrometeor.,* **9,** 622–640.

Syed, T. H., V. Lakshmi, E. Paleologos, D. Lohmann, K. Mitchell, and J. Famiglietti, 2004: Analysis of process controls in land surface hydrological cycle over the continental United States. *J. Geophys. Res.,* **109,** D22105, doi:10.1029/2004JD004640.

Tang, L., and F. Hossain, 2009: Transfer of satellite rainfall error from gauged to ungauged locations: How realistic will it be for the Global Precipitation Mission? *Geophys. Res. Lett.,* **36,** L10405, doi:10.1029/2009GL037965.

Ushio, T., and Coauthors, 2009: A Kalman filter approach to the Global Satellite Mapping of Precipitation (GSMaP) from combined passive microwave and infrared radiometric data. *J. Meteor. Soc. Japan,* **87,** 137–151.

Villarini, G., and W. F. Krajewski, 2007: Evaluation of the research version TMPA three-hourly 0.25°×0.25° rainfall estimates over Oklahoma. *Geophys. Res. Lett.,* **34,** L05402, doi:10.1029/2006GL029147.

Voisin, N., A. W. Wood, and D. P. Lettenmaier, 2008: Evaluation of precipitation products for global hydrological prediction. *J. Hydrometeor.,* **9,** 388–407.